

Effects of linear birefringence and polarization-dependent loss of supermirrors in cavity ring-down spectroscopy

Haifeng Huang and Kevin K. Lehmann*

Department of Chemistry, University of Virginia, Charlottesville, Virginia 22904-4319, USA

*Corresponding author: lehmann@virginia.edu

Received 4 April 2008; accepted 29 May 2008;
posted 23 June 2008 (Doc. ID 94623); published 15 July 2008

In cavity ring-down spectroscopy (CRDS), residual or stress-induced birefringence (10^{-7} – 10^{-6} rad) of supermirrors will lift the polarization degeneracy of TEM_{00} modes and generate two new polarization eigenstates in the cavity with small resonant frequency splitting (~ 0.1 kHz); the new eigenstates are nearly linearly polarized. When both modes are excited simultaneously, the intracavity polarization state will evolve as the energy decays in the cavity. Without polarization analysis, such mode beating would not be observable. However, real supermirrors have a linear polarization-dependent loss (dichroism) that leads to a change in the loss rate as the polarization state evolves and thus to deviation from the expected single-exponential decay. We develop a model for the evolution of the intracavity polarization state and intensity for a cavity with both birefringence and polarization-dependent loss in the mirrors. We demonstrate, experimentally, that these parameters (both magnitudes and directions) can be extracted from a series of measurements of the cavity decay and depolarization of the transmitted light. © 2008 Optical Society of America

OCIS codes: 280.3420, 260.1440.

1. Introduction

Cavity ring-down spectroscopy (CRDS) has proved to be a powerful technique with a broad range of applications in both fundamental and applied spectroscopies [1,2]. In CRDS, absorption of a sample inside a high-finesse optical cavity is observed by an increase in the decay rate of light trapped in the cavity. The ultrahigh sensitivity of CRDS is based on the low loss, a few parts in 10^6 , of the highest-quality dielectric mirrors (so called supermirrors) and the ability to detect a small change, of the order of 1 part in 10^4 , in the decay rate of the cavity. Because the information comes from the rate of decay of optical power, the method is largely immune to fluctuations of the incident laser intensity. The ability to realize very low fluctuations in the extracted cavity decay rate depends on the fact that the cavity decay follows a sin-

gle-exponential (first-order decay) to high accuracy over at least four or five cavity decay times. The introduction of continuous wave (CW) lasers to excite the CRDS cavity has improved sensitivity, because this allows for cleaner and more reproducible excitation of a single TEM_{00} mode of the cavity [3–5]. In previous work [6], we demonstrated that small levels of astigmatism will split the cylindrical degeneracy of higher-order transverse modes and that the resulting mode beating is detectable because the mirrors have a spatial variation in their transmission and reflectivity. With such spatially dependent loss, the different transverse modes are no longer orthogonal [7] (as they are for homogeneous mirrors neglecting diffraction), and as a result multiple-mode excitation leads to mode beating modulations on even an ideal optical detector. Such modulations increase the fluctuations in the extracted cavity decay rate and thus decrease sensitivity.

Even the TEM_{00} modes of linear optical cavities have a degeneracy due to polarization state of the

light. For a nonlinear optical cavity (such as a ring cavity) this degeneracy is lifted because of different phase shifts on reflection for *S* and *P* polarization. It has long been recognized that even the best supermirrors contain some residual birefringence in the coatings (measured to be of the order of microradians per reflection) [8,9] and also that the mounting of the mirrors can introduce additional strain birefringence into the coatings [9]. Different methods [10,11] have been proposed to measure this ultrasmall birefringence of supermirrors. Such birefringence leads to a lifting of the TEM₀₀ mode degeneracy into a pair of orthogonally polarized eigenmodes [10,12] that are in general elliptically polarized and are separated in angular frequency by the net round-trip birefringence (in radians per pass) times the cavity free spectral range [12,13]. For the lowest-loss mirrors, the birefringence (in radians per round trip) is significantly less than the round-trip fractional power loss of the mirrors, and this implies that the splitting of the two polarization modes are less than the resonance width of each mode. For weak birefringence, the polarization eigenstates are nearly linearly polarized [8]. Cavities with mirror birefringence were reviewed previously in [14].

Such a birefringence model, however, should not result in any detectable mode beating effects as long as there is no polarization dependence of the detection after the cavity. Physically, the birefringence is changing the polarization state as the light intensity decays (unless the polarization of one of the eigenmodes has been used for excitation), but this does not change the rate of power decay. We have observed, however, that we often find that the cavity decay rate does contain a polarization dependence that is much higher than the noise in the decay rate. We believe that a polarization dependence of the optical loss (linear dichroism), such as could naturally arise from scattering loss by anisotropic defects in the coatings, must be invoked to explain this observed dependence of the cavity loss on input polarization state. This polarization dependence is not simply a matter of academic interest, as it can lead to instrument baseline drift if the polarization state of the input is not held constant. This can especially be a problem if the light used to excite the cavity is propagated on a non-polarization-maintaining, single-mode optical fiber. Note that polarization maintaining (PM) single-mode fiber does not act as a polarizer but rather has a large birefringence. As a result, mixed single-mode, PM fiber systems, or even all PM systems if the input radiation is not highly aligned with the fast or slow axis of the PM fiber, have even higher temperature drifts in the output polarization state than all single-mode fiber systems. Although polarization-dependent absorption of the medium in a high-finesse cavity has previously been reported [14–16], we know of no previous analysis of the effects of polarization-dependent loss (linear dichroism) of supermirrors on a high-finesse optical cavity. Clearly, in the presence of such loss, mirror birefringence will produce detectable

changes in the cavity power decay, since a changing intracavity polarization state will lead to a changing loss rate. As a result, both polarization-dependent loss and birefringence of the mirrors must be considered simultaneously.

In this paper, we will present the results of a series of measurements we have made on a CRDS cavity that is optimized for methane detection using 1.65 μm absorption. We will also present an analysis based upon Jones matrices [17] to model both birefringence and polarization-dependent loss, each with its own principle axis. In Section 2, the modifications of our previously described experimental setup are given. In Section 3, experimental details and results will be presented. In Section 4, the experimental results will be fitted by the model to determine the polarization-dependent loss and birefringence of the mirrors in our cell. The last section will conclude the paper with a summary and discussion of the significance of our results.

2. Experimental Setup

The CW CRDS setup in our lab was described in detail in previously published papers [6,18]. Here we describe only the modifications made related to the birefringence experiments. Figure 1 is the diagram of our setup. In our previous work [6], the 2.54 cm diameter mirrors of the CRDS cavity were mounted 10.8 cm (to the mirror center) above the optical table, each on a 6 mm thick brass plate that was itself pressed against a 1.2 cm thick brass plates bolted to the laser table. One consequence was that evacuation of the cavity produced a force of 51.7 N against each plate. This caused the mounting plates to deflect, changing the cavity length and effecting the alignment. Modeling the mirror plates as cantilevers and assuming a Young's modulus of 120 GPa for brass, we estimate the displacement of the mirrors as 13 μm and an angular rotation of 1.7×10^{-4} rad. We have added a 0.95 cm thick steel bar connecting the upper parts of two mirror mounting plates. Now, the changing force created by evacuation of the cavity is restricted by the compression strength of the steel. Based on a Young's modulus of 200 GPa for steel, we

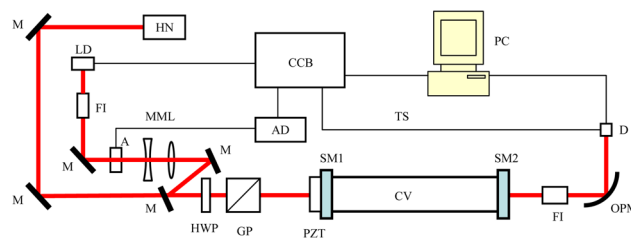


Fig. 1. (Color online) Setup diagram. Red (thick) lines indicate light, and unlabeled black (thin) lines are signal propagation. A, acousto-optic modulator; AD, acousto-optic modulator driver; CCB, control circuit board; CV, cavity; D, detector; FI, Faraday isolator; GP, CPAD polarizer; HN, He-Ne laser; HWP, half-wave plate; LD, laser diode; M, mirror; MML, mode matching lenses; OPM, off-axis parabolic mirror; PC, computer; PZT, three piezo transducers; SM1, front supermirror; SM2, back supermirror; TS, trigger signal. The Pockels cell is not shown here.

can estimate a maximum displacement of 0.17 μm for each thicker brass plate.

The second modification to the system is that the output mirror of the cavity is now rotatable around the optical axis of the cavity. This is realized by putting the flange holding the mirror into an aluminum circle, which has an inner diameter slightly larger ($\sim 200 \mu\text{m}$) than the outer diameter of the flange. The circle is glued onto the brass plate, which previously held the flange with four screws. The orientation angle of the back mirror can be measured with the scale on the circle and the pointer labeled on the flange holding the mirror. The vacuum of the cavity is sealed by an o-ring compressed between the flange and the 6 mm thick brass plate. Unfortunately, we have to vent the cavity to atmosphere pressure each time we wish to rotate the mirror. After the rotation, the cavity is pumped down to vacuum again by a mechanical pump. Because we suspected stress on the mirrors might cause some of the observed mirror birefringence, we also performed the same experiments with the cavity filled to 1 atm pressure by nitrogen gas flow and with all the tightening screws holding both mirrors loosened. Under the low-stress conditions, the flange and the plate holding the back mirror are not pressed against each other, making the rotation of the back mirror much easier. After each rotation, the cavity is realigned by only adjusting the back mirror angle, using a coaxial He–Ne laser beam as a guide. The input beam alignment is then adjusted to reoptimized mode matching into the cavity (by minimizing the transmission of higher-order transverse modes) without adjusting the cavity further. Although the process will guarantee that the optical axis of the cavity strikes the same area on the front mirror, the axis will hit different points on the back mirror for each rotation because the rotation center of the back mirror does not precisely overlap the optical axis of the cavity. We could not practically rotate the input mirror because of its wedge (0.5°), which would require substantial realignment of the input beam as the input mirror is rotated.

The cavity is excited with radiation from a distributed feedback, fiber pigtailed semiconductor diode laser (NTT Electronics Corporation, NLK1U5EAAA). Right after the collimated optical fiber output, the 1652 nm laser passes one external optical isolator (IsoWave, I-15-UHP-4), with a measured isolation of 47 dB at 1652 nm. The output polarizer of the isolator ensures that the light incident on the cavity is linearly polarized in a fixed direction. The beam is then mode matched and focused on the flat input mirror of the cavity. To control the direction of polarization of the light incident on the cavity, we used a zero-order half-wave plate (CVI, QWPO-1550-05-2-R10) and polarizer (CVI, CPAD Glan laser polarizer with extinction ratio 5×10^5), both mounted on rotatable mounts. The second polarizer we used to keep a high degree of linear polarization. In some of the experiments, we generated circular polarized light to excite the cavity by replacing the polarizer with a Pockels

cell (Quantum Technologies, LN-9) with a voltage of 3.1 kV, at which the Pockels cell acts as a quarter-wave plate.

For some measurements, a second isolator (IsoWave, I-1550-4, with isolation of 35 dB at 1652 nm) was placed in the optical path between the output mirror and the detector. This isolator is mounted on a rotatable mount. This isolator serves two purposes. One is that it has an input polarizer that analyzes the polarization state of the light leaving the optical cavity. The second is to reduce any feedback to the cavity from the surface of the detector. While the window and front surface of the detector are tilted off axis to prevent a direct specular reflection back into the TEM_{00} mode of the ring-down cavity, scattered light from the detector can feed back into the cavity and change the cavity decay rate [2]. Because of interference, such feedback of power must be below -80 dB to bury the resulting changes in cavity decay rate in our present cavity decay rate noise (which has a fractional value of $\sim 10^{-4}$). In our experiments, the cavity length is modulated to achieve resonance of the input laser with a resonance mode of the optical cavity by applying a triangle wave to three piezoelectric transducers. When the cavity transmission intensity exceeds a preset threshold, the input radiation is turned off (with 49 dB extinction ratio) in less than 1 μs by blocking the RF radiation used to drive an acousto-optic modulator (IntraAction, ACM-802AA14) that otherwise deflects light into the cavity. The distance between the mirrors is 39.5 cm, which implies a cavity free spectral range (FSR) of 379.5 MHz. Each cavity decay transient is captured at 10^6 samples/s by a 12 bit digitizer, and the cavity decay time, τ , is extracted by a non-linear least squares fit.

3. Experimental Results

Before we present our results, we want to describe the xyz coordinate system used in this paper, which is shown in Fig. 8 below. x is vertical, y is horizontal, and z is the direction of light propagation. The positive direction of an angle is from the x to the y axis, with the x axis defined as 0° . All the angles in this paper have been transformed to this scale.

In the first experiment we discuss, we excited the cavity with circularly polarized light and used the optical isolator as analyzer after the cavity. Since, as the analysis presented below will show, the two eigenpolarization modes are nearly orthogonally linearly polarized, the use of circularly polarized input radiation ensures that we get similar excitation amplitudes in each of these modes. We measured the cavity decay time constant, both mean value and fluctuations, as a function of polarization analyzer angle. These measurements were repeated as the back mirror orientation angle was rotated from -273° to 87° , with a rotation step of 20° . Only by rotating one cavity mirror relative to the other could the individual contributions of the mirrors to the birefringence and polarization-dependent loss be

determined. We observed that for each back mirror orientation angle, there exist two perpendicular angles of the analyzer for which the system has the quietest decay signal, i.e., the smallest standard deviation of τ for an ensemble of 80 successive decay signals. This is true for both an evacuated cavity and the low-mirror-stress conditions. When the cavity is under vacuum, if the analyzer is rotated modestly from either of these two angles, the extracted decay time will become noisier, with larger standard deviation of the fitted τ values. If the post cell isolator is rotated further away from these two angles, every decay signal will contain mode beating noise, with reduced τ^2 for the fit [6] of the decay to a single-exponential decay much larger than 1 (decay transients with reduced τ^2 larger than 60 have been observed). This arises from the beating of the two eigenpolarization modes. The beating frequency reflects the frequency splitting of these two modes, which in turn is determined by effective round-trip birefringence of the cavity. For each back mirror orientation angle, these two isolator angles are independent of the polarization state of the incident light. If the incident light is linearly polarized and the decay signal at the detector is strong enough, the same value of these two angles can be obtained, though in that case the relative excitation intensity of the modes will scale as $\cos^2(\theta)$, where θ is the angle between the input polarization direction and polarization direction of the eigenpolarization mode. For the cavity under low-stress conditions, however, the reduced τ^2 can be much smaller than that with the cavity under vacuum because of smaller the birefringence obtained by releasing the stress on mirrors. Figure 2 was recorded with the cavity under low-stress conditions. It shows how τ and the stan-

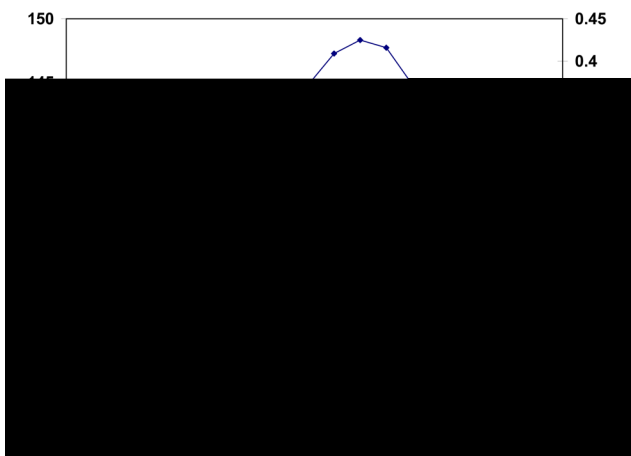


Fig. 2. (Color online) τ (right vertical axis) and the standard deviation of τ (left vertical axis) change in the angle of the polarization analyzer at the output of the cell. This data was recorded when the back mirror was at -53° and the cavity was under low-stress conditions. The cavity was excited by circularly polarized light. The two angles of quieter data are indicated by the two arrows. Because of the low-stress conditions, no decay signal with reduced τ^2 larger than 1.5 was recorded, which is the criteria for bad decay in the experiments.

dard deviation of τ change as a function of analyzer orientation angle. We can see that the value of τ from single-exponential fitting is different for detection on each of the eigenpolarization directions. This difference reflects the net round-trip polarization-dependent loss, as will be discussed below. We also found that these two eigenpolarization angles change with the orientation angle of the back mirror and have a period of 180° . While this is what is expected, it provides confirmation that the birefringence is not highly localized on the mirrors as the spot sampled by the TEM_{00} mode unfortunately moves as we rotate the mirror. Figure 3 shows how these eigenpolarization mode directions follow the rotation of the back mirror when the cavity is under vacuum. Figure 4 shows how they change when the cavity is under the low-stress conditions. We can see these two angles behave very differently under these two conditions, indicating the influence of strain-induced birefringence in the coatings.

In the second experiment, the Pockels cell was replaced by a polarizer and the isolator behind the cavity was removed. Without the isolator, the standard deviation of τ is close to that measured when the isolator is at one of the two eigenpolarization angles, and, more important, no cavity decays with reduced τ^2 much larger than one for the exponential decay were recorded, indicating weak mode beating effects even when both modes were excited simultaneously. We found that τ changes as a \sin^2 function of the angle of incident linearly polarized light. The result is shown in Fig. 5. With the rotation of the back mirror, not only do the angles corresponding to the maximum or minimum of τ shift, but the mean τ and its modulation amplitude [$= (\tau_{\max} - \tau_{\min})/2$] changes substantially. Figure 6 shows how the modulation amplitude and the polarization angle corresponding to the maximum of τ change with the back mirror rotation. We believe that this lack of smooth angular dependence arises from the importance of localized defects on the mirror surface (which can be seen visually under a microscope [6]). However, the change

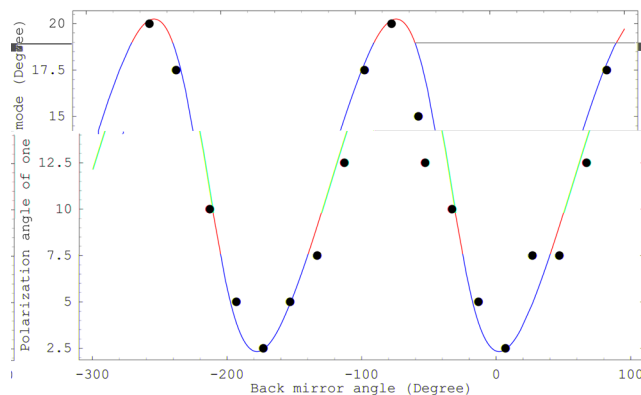


Fig. 3. (Color online) The polarization plane of one of the two modes changes with back mirror rotation angle when the cavity is under vacuum. The other mode (not shown here) is perpendicular to the one in this figure. The points are measured results, and the curve is calculated from Eq. (7) with $\tau_1 \approx 3.3 \tau_2$.

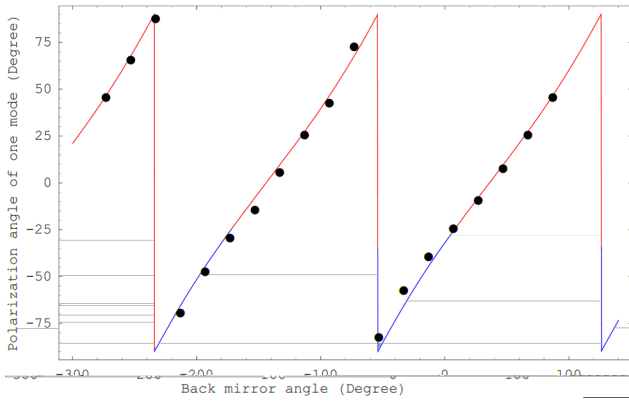


Fig. 4. (Color online) The polarization plane of one of the two modes changes with back mirror rotation angle when the cavity is under low-stress conditions. The other mode (not shown here) is perpendicular to the one in this figure. The points are measured results, and the curve is calculated from Eq. (7) with $\tau_1 \approx 1/6 \tau_2$. The discontinuity in the curve arises because the angle is defined between $-\pi/2$ and $\pi/2$.

of the polarization angle of the maximum τ is much smoother than that of the modulation amplitude. For each back mirror angle, the two analyzer angles that produce quiet decays do not match the incident polarization angles corresponding to the maximum or minimum of τ values. This reflects that the fast and slow axes for the net round-trip birefringence

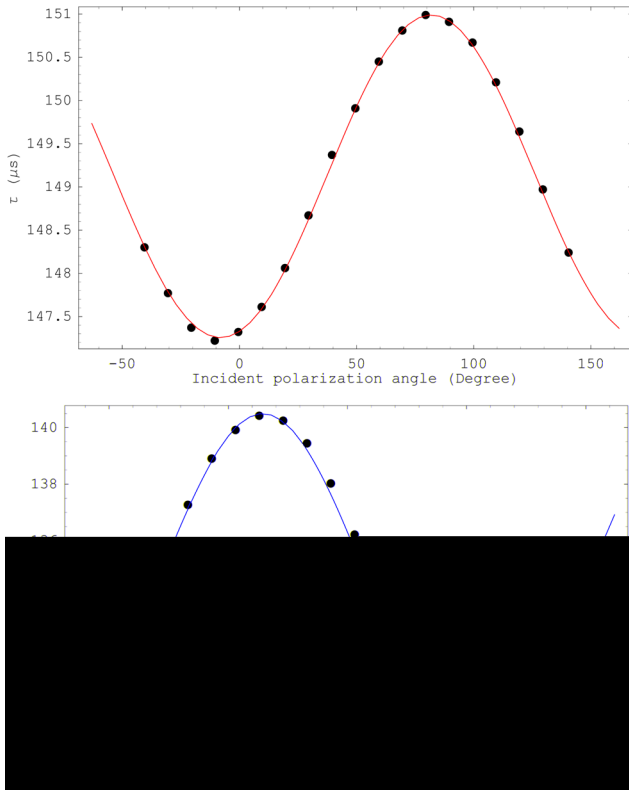


Fig. 5. (Color online) τ from single-exponential fitting changes as a sine function of the polarization angle of the incident laser. The dots are experimental data, and the curves are calculated from Eq. (21). Back mirror angles are (top) 7° and (bottom) -53° with the cavity under vacuum.

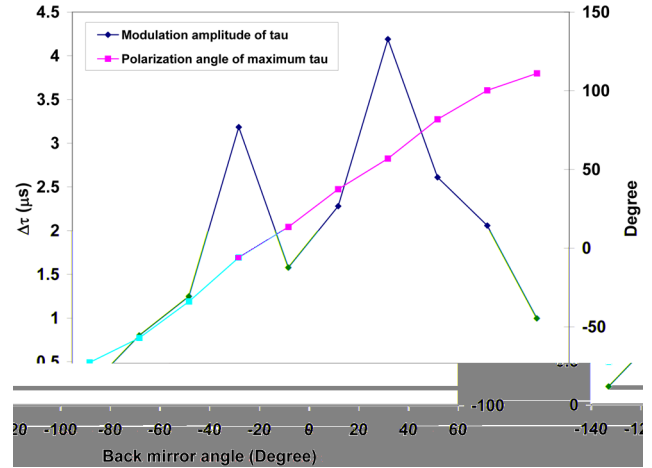


Fig. 6. (Color online) Modulation amplitude of τ (blue jagged curve, left vertical axis) and the polarization angle corresponding to maximum τ (smooth pink curve, right vertical axis) for each orientation angle of the back mirror. The cavity was under vacuum. The back mirror was rotated from -133° to 47° with a step size of 20° .

do not match those of min and max loss. Similar results have been obtained with the cavity under the low-stress conditions.

In the third experiment, the isolator was put back behind the cavity. Before the experiment, the polarization angle of the CPAD polarizer on the input beam and that of the input polarizer of the isolator were calibrated with the same linearly polarized light. The extinction ratio of the isolator was measured to be close to that of the cavity input polarizer. In this experiment, the back mirror was turned to certain angle. Then the input polarization and analyzer polarization directions were rotated synchronously, with the two polarizers crossed. This is equivalent to the situation in which the polarizer is fixed at the x axis and the isolator is at the y axis, while the cavity is rotated around the optical axis in the opposite direction. The cavity length was scanned over one free spectral range, and the transmission was averaged on a digital oscilloscope. We also measured the averaged transmission of the cavity when both polarizers were aligned. This allows the degree to which the cavity depolarizes the input light signal [19] to be quantitatively measured. We found that this depolarization ratio is also a sine function of the rotation angle of the CPAD polarizer, with a period of 90° . Figure 7 was recorded when the back mirror was at 62° . It shows that this effect becomes much smaller when the stress on the mirrors is released.

4. Discussion

Figure 8 shows the schematic of the optical cavity. The residual and stress-induced birefringence of each supermirror is modeled as a very thin wave plate on top of the high-reflectivity coating of the mirror, as shown by the inset at the upper left corner of Fig. 8. The single-pass phase retardances of both mirrors are τ_1 and τ_2 . On each reflection from the mirror,

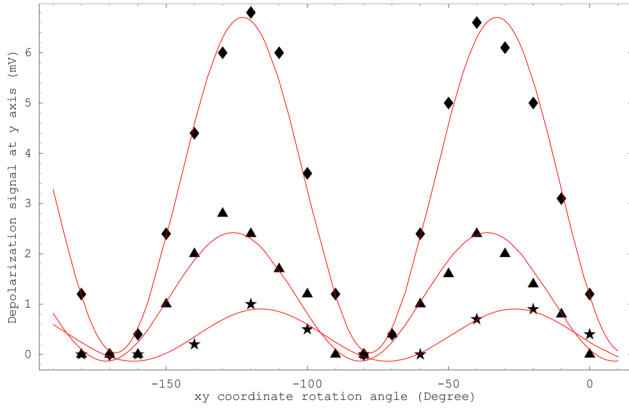


Fig. 7. (Color online) The light intensity at the y axis $|E_y^{\text{out}}|^2$ is a sine function of the rotation of the xy coordinate. The curves are theoretical predictions. Diamonds, vacuum cavity, fitted to the expression $(3.37 + 3.33 \sin[(\theta)/45 - 2.41])$ mV. Triangles, 700 torr cavity pressure and screws not loosened, fitted to the expression $(1.14 + 1.28 \sin[(\theta)/45 - 2.18])$ mV. Stars, low-stress conditions, fitted to the expression $(0.38 + 0.52 \sin[(\theta)/45 - 2.86])$ mV. Here θ is the rotation angle of the xy coordinate degrees. $|E_x^{\text{out}}|^2$ is 200 mV, measured when the system was not triggered for decay signal and both polarization angles of the polarizer and isolator were aligned.

the light will pass through the wave plate twice. The angles between the slow axes of the two mirrors and the x axis are α_1 and α_2 , respectively. The fast axes of both mirrors are perpendicular to the two corresponding slow axes. If we assume that the reflectivity of both mirrors is no longer isotropic, the polarization-dependent loss of both mirrors can be described by the two parameters $r_{i \max}$ and $r_{i \min}$, $i = 1$ and $i = 2$, which are the maximum and minimum electric field reflectivity, respectively. The angles between the directions of maximum reflection and the x axis are β_1 and β_2 for the cavity mirrors. The directions of minimum reflection are perpendicular to those of the corresponding maximum reflection.

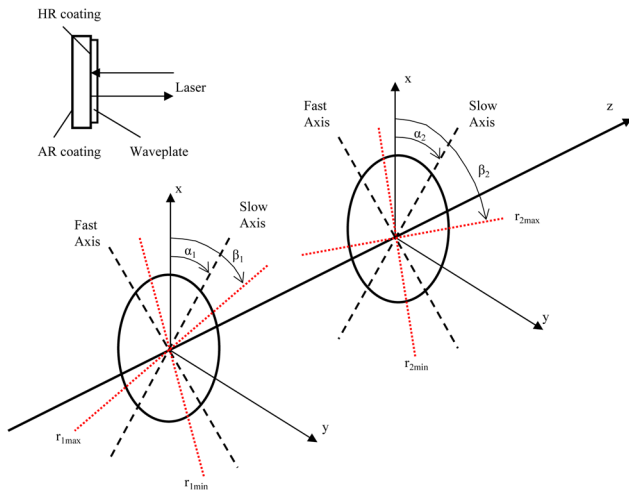


Fig. 8. (Color online) Physical picture of the experiment. Inset (upper left corner), schematic diagram of the mirror model.

We can model the polarization state as the optical beam propagates inside the cavity by using Jones matrices [17]. Let the rotation matrix $R(\theta)$ be defined as

$$R(\theta) = \begin{pmatrix} \cos(\theta) & \sin(\theta) \\ -\sin(\theta) & \cos(\theta) \end{pmatrix}. \quad (1)$$

Here θ is the rotation angle. In the following equations, the index i is always 1 (input mirror) and 2 (output mirror). The Jones matrices for reflection from either mirror are given by

$$G_i = a_i R(-\theta_i) \begin{pmatrix} 1 + b_i & 0 \\ 0 & 1 - b_i \end{pmatrix} R(\theta_i) \quad (2)$$

with definitions

$$a_i = \frac{r_{i \max} + r_{i \min}}{2}, \quad b_i = \frac{r_{i \max} - r_{i \min}}{r_{i \max} + r_{i \min}}. \quad (3)$$

Note that r denotes electric field reflectivities, the square root of the power reflectivity value that is usually quoted. For each pass of the thin wave plate on either mirror, the Jones matrices are [20]

$$F_i = R(-\theta_i) \begin{pmatrix} \exp(j\theta_i/2) & 0 \\ 0 & \exp(-j\theta_i/2) \end{pmatrix} R(\theta_i), \quad (4)$$

with $j^2 = -1$. For each complete reflection of light from either mirror, the net Jones matrix is

$$M_i = F_i G_i F_i. \quad (5)$$

Corresponding to a round trip of the light in the cavity, the Jones matrix is defined as

$$M = M_1 M_2. \quad (6)$$

We can exploit the fact that b_i and θ_i are $\ll 1$ to expand and keep only the terms linear in these small numbers to get

$$M = a_1 a_2 \begin{bmatrix} \left(\begin{matrix} 1 & 0 \\ 0 & 1 \end{matrix} \right) + \left(\begin{matrix} b \cos(2\theta) + j \cos(2\theta) & b \sin(2\theta) + j \sin(2\theta) \\ b \sin(2\theta) + j \sin(2\theta) & -(b \cos(2\theta) + j \cos(2\theta)) \end{matrix} \right) \end{bmatrix}, \quad (7)$$

where we have net round-trip polarization-dependent loss parameters and birefringence values

$$b^2 = b_1^2 + b_2^2 + 2b_1 b_2 \cos(2(\alpha_1 - \alpha_2)), \quad (8)$$

$$= \frac{1 + \alpha_2}{2} + \frac{1}{2} \tan^{-1} \left(\frac{b_1 - b_2}{b_1 + b_2} \tan(\alpha_1 - \alpha_2) \right), \quad (9)$$

$$\alpha^2 = \frac{\alpha_1^2}{1} + \frac{\alpha_2^2}{2} + 2 \alpha_1 \alpha_2 \cos(2(\alpha_1 - \alpha_2)), \quad (10)$$

$$= \frac{1 + \alpha_2}{2} + \frac{1}{2} \tan^{-1} \left(\frac{1 - \alpha_2}{1 + \alpha_2} \tan(\alpha_1 - \alpha_2) \right). \quad (11)$$

Note that b varies from $b_1 + b_2$ to $|b_1 - b_2|$ as $\alpha_1 - \alpha_2$ varies from 0 to $\pi/2$. The direction of maximum polarization loss is always between α_1 and α_2 , being closer to the α_i direction of the larger b_i . The same comments apply to the net round-trip birefringence and the direction of its slow axis. The fractional errors in the round-trip Jones matrix of this first-order treatment are of the order of b^2, α^2 , which are negligible for the mirrors used in CRDS experiments.

Optical elements can also have circular birefringence (different index for left- and right-handed circularly polarized light, i.e., optical rotation) and differential loss for different circularly polarized light (circular dichroism). These have Jones matrices in the same form as Eqs. (4) and (2), respectively, but expressed in the left- (L) and right- (R) handed polarization basis instead of the linear polarization basis. Physically, such effects arise from chiral coatings or defects, such as helical coatings that could arise from deposition at an angle to the normal in an optic that is rotated during the deposition. A key difference from the linear case is that reflection reverses optical chirality, i.e., interchanges the L and R polarization bases. Including this interchange, we find that circular birefringence exactly cancels the inward and outward transmission through a layer of the coating. The circular dichroism cancels to first order and to second order is indistinguishable from first-order linear dichroism. Thus, we do not expect mirror circular birefringence and dichroism to play a significant part in polarization dependence in CRDS. Hall *et al.* [9] report that “for almost all (super) mirrors” the residual circular birefringence is at least an order of magnitude smaller than residual linear birefringence. For a sample contained between the mirrors, observation of optical rotation has only been observed by insertion of a 1/4 wave plate before each mirror, which undoes the optical chirality change of the mirror reflection [21].

An external magnetic field can also induce birefringence of the mirrors by the Faraday effect, and this adds instead of subtracts upon retroreflection (the principle of an optical isolator). Estimating the Verdet constant of fused silica at 1.65 μm as 0.25 $\text{rad m}^{-1} \text{T}^{-1}$ (from Tan and Arndt [22] and using their observed scaling with dn/d to predict the near-IR value), and recognizing that the mean penetration of the light into the dielectric mirror is $\sim \lambda/4$, we can predict that an Earth field of $\sim 10^{-5} \text{T}$ will generate a rotation of the order of $4 \times 10^{-12} \text{rad}$ per reflection, many orders of magnitude lower than the residual birefringence we measure and thus negligible.

Birefringence and dichroism in the mirror substrates will not lead to polarization changes during the ring down (since detected light transits each substrate once regardless of the detection time). Thus,

we can ignore any such effect, though if it were large for the input or output mirror, it would compromise the polarization selectivity of the cavity excitation or analysis of the cavity output, respectively. The only measurement that we have made that is directly influenced by the mirror substrates is the cavity depolarization. It is worth noting that for our mirrors, the total optical path length in the coating, at one cavity decay time, dwarfs the path in the mirror substrate, so we do not believe that the substrate depolarization is significant in our measurements.

The round-trip matrix M has a pair of eigenvalues λ_1 and λ_2 and two corresponding eigenvectors,

$$\lambda_{1,2} = a_1 a_2 (1 \pm [b^2 - \alpha^2 + 2jb \cos(2(\alpha_1 - \alpha_2))]^{1/2}). \quad (12)$$

With both birefringence ($\alpha \neq 0$) and polarization-dependent loss ($b \neq 0$), λ_1 and λ_2 are no longer complex conjugates of each other.

The resonant frequency of the cavity is determined by the round-trip phase shift of the light in the cavity. Therefore, the frequency splitting of the eigenpolarization directions for each TEM_{00} mode is given by [12,13]

$$\begin{aligned} &= \frac{\arg(\lambda_1) - \arg(\lambda_2)}{2} \text{FSR} \\ &\approx \frac{c}{2L} \frac{1}{\mathfrak{I}} ([b^2 - \alpha^2 + 2jb \cos(2(\alpha_1 - \alpha_2))]^{1/2}), \quad (13) \end{aligned}$$

where c is the speed of light, L is the cavity length, \approx refers to the limit of small b and α (i.e., use of the first-order expansion), and $\mathfrak{I}(\dots)$ is the imaginary part of its argument. Note that there would be no mode splitting without net birefringence (i.e., $\alpha = 0$) and that for zero net polarization-dependent loss (i.e., $b = 0$) the mode frequency splitting is FSR/α . For $b < \alpha$, the splitting is reduced, but typically modestly so. For $b = \alpha$, the splitting is $\sqrt{|\cos(2(\alpha_1 - \alpha_2))|} \text{FSR}/\alpha$. It hardly changes for larger b . In our system, α_1 and α_2 are of the order of 10^{-6}rad or less (see the latter part of this section). If $\alpha_{\text{max}} - \alpha_{\text{min}}$ in the second experiment is 5 s, b_1 and b_2 are of the order of 10^{-8} , and $1 - a_1$ and $1 - a_2$ are of the order of 10^{-6} for $\tau \geq 130$ s. Therefore, α will be about 0.1 kHz. This is much smaller than the linewidth of the TEM_{00} mode, which is about 1 kHz for $\tau = 150$ s. Put in a time domain picture, the beating period is much longer than the cavity decay time; so only a small fraction of one period will be observed. This can distort the shape of the decay, leading to an increased reduced χ^2 of the fit, but no obvious beating will be visible in the decay.

In general, these two eigenvectors of polarization will not be orthogonal, since they are eigenvectors of a non-Hermitian matrix [7]. The overlap of these two states is closely related to how strong the mode beating effect is in the decay signal. For $b = \alpha$, the magnitude of the overlap of the two eigenvectors ap-

proaches unity as $\beta \rightarrow \pi/4$. However, in this limit, the matrix M^2 approaches a constant times the identity matrix, and thus there is no accumulation of phase due to either birefringence or polarization-dependent loss during the ring down. More generally, the modes are always orthogonal when β is a multiple of $\pi/2$ and a maximum for odd multiples of $\pi/4$. The maximum value of the magnitude of the mode overlap is b/β for $b \ll \beta$ and vice versa in the opposite limit. Likewise, the modes will not generally be linearly polarized; the ellipticity of the eigenpolarization modes qualitatively following the mode overlap. In the first-order theory we are using here, the eigenpolarization modes are linearly polarized if $b = 0$. Going to higher order, this is no longer true. However, despite this, the first-order approximation still gives a clear physical pictures of our results.

A strong ellipticity of the eigenmodes appears to imply that the output of the cavity will be strongly depolarized. However, this is not the case as long as the round-trip loss is much higher than either the round-trip birefringence or polarization-dependent loss. Physically, this is because most of the light inside the cavity has decayed by the time the polarization state has been significantly affected. For the case of only birefringence, if the input to the cavity at time $t = 0$ is linearly polarized with angle θ , the intensity of the light perpendicular to the initial direction at time t is $I_{\perp}(t) = I_{\parallel}(0) \exp(-t/\tau) \sin^2(2(\theta - \theta_0)) \sin^2(\text{FSR} t)$. Averaged over the decay, for $\text{FSR} \tau \ll 1$, the fractional power transferred into the component perpendicular to the input will be $2(\text{FSR} \tau \sin(2(\theta - \theta_0)))^2$. Likewise, with only polarization-dependent loss, the perpendicular output intensity will be $I_{\perp}(t) = I_{\parallel}(0) \exp(-t/\tau) \sin^2(2(\theta - \theta_0)) \sinh^2(b \text{FSR} t)$. Again, for $b \text{FSR} \tau \ll 1$ the time-averaged fractional power transmitted into the perpendicular component will be $2(b \text{FSR} \tau \sin(2(\theta - \theta_0)))^2$. For elliptically polarized eigenmodes, there will be no input linear polarization that will not experience some depolarization, but the magnitude of the depolarization will not be increased. In our experiments, $\text{FSR} \tau \sim 0.06$ for $\tau = 150$ s.

In our experiments, the ratio b/β is of the order of 10^{-2} – 10^{-1} . The overlap of the two eigenpolarization modes is also of this order. With the 0.1 kHz splitting between these two modes, if there is no analyzer behind the cavity, it will not cause an observable mode beating effect in the ring-down signal because the modulation depth, which is of the order of the overlap, is small. However, when both modes are equally excited by circular polarization light, a polarization analyzer behind the cavity can increase this modulation depth to close to unity, causing an observable mode beating effect on the cavity decay; the ring-down signal deviates significantly from a single-exponential decay, and thus the reduced χ^2 will be much larger than 1. This mode beating is very sensitive to the mode splitting $\Delta\omega$. When the analyzer is turned to those two good angles, because these two eigenpolarization modes are very close to linearly po-

larized states, the analyzer will only detect one of the two eigenmodes and remove the mode beating effect. This is confirmed by the results of our first experiment. Because the mode overlap is small, these two states can be regarded as orthogonal to each other, corresponding to the result that these two good angles of the isolator are perpendicular to each other.

When the back mirror rotates, both θ_1 and b will change. From Fig. 6, we can see that b strongly depends on the local condition of the spot on the back mirror, and the TEM_{00} mode hits different spots for different back mirror angles. This means that both the magnitude and the orientation of the polarization-dependent loss of the back mirror change with its rotation. However, if b is much smaller than β , the rotation behavior of the orientations of these two polarization states is determined mainly by the ratio of θ_1 to θ_2 and by directions of the two slow axes (θ_{1s} and θ_{2s}). A simulation demonstrates that the data in Fig. 3 can be reproduced if $\theta_1 \approx 3.3 \theta_2$. With this assumption, when the back mirror rotates, the polarization angles of two mode oscillate around the slow axis and the fast axis of the front mirror, respectively, as shown in Fig. 3. The data in Fig. 4 can be reproduced if $\theta_1 \approx 1/6 \theta_2$. With this condition, the rotation of the polarization angles of both modes is determined mainly by the back mirror rotation. Both angles will follow the back mirror rotation from 0° to 360° , as shown in Fig. 4. The discontinuity in the curve is because the angle is defined between $-\pi/2$ and $\pi/2$. When $\theta_1 = \theta_2$, if b_i is much smaller than β_i , the polarization angle of both modes will linearly increase by half of the back mirror rotation angle. Both Figs. 3 and 4 show only the polarization angle of one of the two modes. The angle of the other mode is measured to be perpendicular to the one shown in both figures. In Fig. 3, the median angle of this oscillation (vertical axis) corresponds to the angle of the slow (or fast) axis of the front mirror, which is about 11.3° . When the back mirror is at about 56.3° , both slow axes of the mirrors are aligned. From Fig. 4, however, we can only determine the orientation of the slow axis of the back mirror, because both polarization angles of the two modes are determined mainly by the orientation of the back mirror (imagine the extreme situation of $\theta_1 = 0$). When the back mirror is at about 36° , the slow (or fast) axis of the back mirror is along the x axis, i.e., vertical. Figures 3 and 4 suggest that the directions of both slow axes change with the stress condition of the mirrors. When both slow axes are aligned, those two polarization angles of quietest ring-down signal correspond to the directions of the slow axis and the fast axis of both mirrors.

In the third experiments, the depolarization degree of the cavity under different conditions is measured, which allows us to determine the magnitude of the effective cavity round-trip birefringence. The back mirror is at a 62° angle. If the incident laser is linearly polarized at the x axis with amplitude E_x^{in} , because of the birefringence and polarization-dependent loss of both mirrors, the output light of the cavity will contain polarization components of

both x and y axes. The intensity ratio between the y component and the x component is defined as [8]

$$= \frac{|E_y^{\text{out}}|^2}{|E_x^{\text{out}}|^2}. \quad (14)$$

The transmission Jones matrix T of the cavity can be written as

$$T = T_2 \sum_{n=0}^{\infty} [\exp(j(2n+1)\phi) M^n] T_1. \quad (15)$$

T_1 and T_2 are Jones matrices of the transmission of both mirrors. $\phi = kL$ is the phase shift per pass of the cavity. k is the wave vector of the laser. If we ignore the anisotropy of the transmission of both substrates and both mirrors, we can write according to the above equations:

$$= \frac{F^2}{2} [(a_1 \sin(2\phi_1) + a_2 \sin(2\phi_2))^2 + (b_1 \sin(2\phi_1) + b_2 \sin(2\phi_2))^2]. \quad (16)$$

Because b_i is much less than a_i for this back mirror angle, we can ignore the depolarization contribution from b_i and simplify further to

$$= \frac{\frac{2F^2}{2} (1 + f^2 + 2f \cos(2\phi))}{2} [1 + \sin(4\phi_1 + \phi)]. \quad (17)$$

$F = 1/(1 - a_1 a_2)$ is the finesse of the cavity, $f = a_1/a_2$, and $\phi = \phi_2 - \phi_1$; ϕ is a phase angle. From the above equation, ϕ is a sine function of $4\phi_1$, as demonstrated in Fig. 7. Figure 7 also shows that the stress was only partly released when the cavity pressure increased from vacuum to 700 torr. After the pressure increased to 760 torr and all tightening screws were loosened, the stress was reduced further. With the knowledge of the relative ratio between ϕ_1 and ϕ_2 and from the earlier experiments, we can calculate the absolute values of both phase retardances by fitting the results in Fig. 7 to Eq. (17). For the cavity under vacuum, ϕ_1 is 1.0×10^{-6} rad and ϕ_2 is 3.1×10^{-7} rad. For the low-stress cavity, ϕ_1 is 0.83×10^{-7} rad and ϕ_2 is 5.0×10^{-7} rad. It is interesting that when the stress was released, ϕ_1 decreased about one order, while ϕ_2 increased about 50%. This may be related to the fact that the back mirror is curved while the front mirror is flat. We did not perform the back mirror rotation experiment when the cavity pressure was 700 torr. Therefore we cannot calculate ϕ_i for that condition. We assume that the ϕ_i values measured under the low-mounting-stress conditions arise from the residual birefringence of high-reflectivity coatings.

The caption to Fig. 7 gives the three equations that fit the observed transmission depolarization. In all three cases, the cell depolarization is essentially zero for $\phi \approx -78^\circ$ and $\phi \approx 168^\circ$, as predicted by Eq. (17), though there is some shift of the minima and maxima

with changes in mirror stress. It is evident that the cavity under vacuum has a higher peak depolarization. When the mounting stress is released, the peak depolarization is substantially reduced, reflecting the reduction in the round-trip birefringence. The average of the two fitting coefficients (essentially half of the peak depolarization) was used to calculate ϕ_i . Zero depolarization signal corresponds to the incident polarization parallel to one of the eigenpolarization directions.

Because of mirror loss, the round-trip matrix M has eigenvalues $|\lambda_i| < 1$. The quantities $1 - |\lambda_i|^2$ correspond to the energy loss per round trip of these two modes in the cavity. The decay time constants of both modes τ_i can be calculated as

$$\tau_i = \frac{-t_r}{2 \ln(|\lambda_i|)}. \quad (18)$$

$t_r = 2L/c$ is the round-trip time; c is the speed of light. With polarization-dependent loss, ϕ_1 and ϕ_2 are no longer equal. Moreover, because the directions of maximum reflection are not necessarily the same as those of the slow axes of the mirrors, the polarization angles of these two modes will not match those of incident light, resulting in the ϕ_{max} and ϕ_{min} measured in the second experiment. When the cavity is excited by linearly polarized light, two modes with different ϕ will be excited simultaneously. The final decay signal is no longer single-exponential decay. When the final decay signal is fitted by a single-exponential decay function, the fitted ϕ will oscillate sinusoidally between ϕ_{max} and ϕ_{min} , as observed in Fig. 5. This fitted ϕ can be calculated approximately if we assume that the depolarization rate of the incident linear polarization light is small compared with the energy decay rate of the cavity (remember $\text{FSR} \sim 0.06$ for our system). The Jones vector of linearly polarized light in the cavity with polarization angle ϕ with respect to the x axis and an intensity of 1 is

$$u = \begin{bmatrix} \cos(\phi) \\ \sin(\phi) \end{bmatrix}$$

and θ_i from the first and third experiments are used. $a_1 a_2 = [1 - t_r / (4 \theta_0)]^2$ and $b = t_r (\theta_{\max} - \theta_{\min}) / (4 \theta_0)$ can be calculated from the experimental results. Here $\theta_0 = (\theta_{\max} + \theta_{\min}) / 2$. The only adjustable parameter in the calculation is θ_i . When $\theta_i \approx \theta_0$, we find that the polarization angles of the two modes are also close to those of θ_{\max} and θ_{\min} (lower part of Fig. 5). If θ_i and θ_0 are not close to each other, as for most of the back mirror angles, the polarization angles of the two modes do not overlap with those of θ_{\max} and θ_{\min} (upper part of Fig. 5). Moreover, with fitted parameters, the calculated polarization angles of the two modes match measured values very well. The calculated θ_1 and θ_2 of the two eigenmodes match those measured only qualitatively, because all the angles in this paper are accurate to about 2° , while θ_i is very sensitive to polarization angles with the existence of polarization-dependent loss. In principle, by performing the incident polarization rotation experiment for four different back mirror angles, we are able to obtain b_i and θ_i for both mirrors. However, as already discussed, it is extremely difficult to guarantee that the TEM₀₀ mode in the cavity hits the same spot on both mirrors as a mirror is rotated. Because of the spatial anisotropy of the mirror reflection, small spatially localized changes of the HR coating will introduce a large shift of θ_i (see how different θ_i is in different figures in this paper). This limits our ability to quantitatively model changes in the cavity decay time as one mirror is rotated with respect to the other. In fact, the polarization angles of θ_{\max} in Fig. 6 are exactly θ_0 , with much smoother changes with mirror rotation than the modulation amplitude of θ_i . When the back mirror rotates 180° (from -133° to 47°), θ_i also changes almost 180° (from -72.6° to 111°), as it should have in the ideal situation that the TEM₀₀ mode always hits the same spots to both mirror. This suggests that although θ_i strongly depends on the local condition of the high-reflection coating of mirrors, the principle axes of the polarization-dependent loss of both mirrors are less locally determined, which in turn implies that the mirror defects causing the largest localized loss have little polarization dependence on their scattering loss. For several back mirror angles, the polarization-dependent loss is slightly larger than normal and of the order of 10^{-7} , such as the data of the lower part of Fig. 5, which shows that there are localized contributions to the polarization-dependent loss.

Lee *et al.* [11] discussed a procedure to determine θ_i by measuring the difference in τ for decays of separated right circularly polarized (RCP) and left circularly polarized (LCP) light leaving the cavity when it is excited by linear polarization. We note that the RCP and LCP states are normally not eigenpolarization states in the cavity. The decay signal of RCP or LCP light should contain a mode beating effect. However, because their τ is so small (~ 15 ns) and the mode splitting is about 0.4 kHz (calculated from [11]), the effects of the mode beating simply result in a slightly larger and smaller decay rate for the RCP and LCP compared with unanalyzed cavity decays. The analy-

sis they presented is justified when $\tau \ll 1$. Reference [11] also did not consider the influence of the polarization-dependent loss of mirrors, which we believe exists for a pair of real supermirrors.

5. Conclusion

In conclusion, we have found that birefringence and polarization-dependent loss of supermirrors in CRDS modify the cavity decay and effect the sensitivity. We have analyzed the cavity including both effects. For each orientation of the cavity mirrors, there exist two special angles of a postcavity optical isolator (polarization analyzer) that are perpendicular to each other and give the most stable ring-down decay rates, as shown in Fig. 2. This can be explained by assuming that birefringence of supermirrors will lift the degeneracy of TEM₀₀ between x and y axes and generate two eigenpolarization states of the cavity. These two states are almost perpendicular to each other and are very close to linearly polarized states. By putting one high-extinction-ratio polarizer in front of the cavity and another behind the cavity, one can selectively excite and detect only one of these two modes, removing the mode beating effect from the ring-down signal and producing the most stable cavity decay rate and thus maximum CRDS sensitivity. When one cavity mirror rotates relative to the other, the rotation of the polarization eigenmodes is determined by the birefringence and polarization-dependent loss together. If the birefringence is dominant, it is determined by the relative ratio between θ_1 and θ_2 , the single-pass birefringences of the two cavity mirrors. Depending on this ratio, this behavior can be very different, as shown in Figs. 3 and 4. By rotating the xy axes, we have measured and quantitatively fitted the depolarization efficiency of the cavity. Combining these two results, the absolute values of both phase retardances are calculated to be of the order of 10^{-7} – 10^{-6} rad, while b_i , the measurement of polarization-dependent loss, is of the order of 10^{-8} . The fact that θ_i changes sinusoidally with the rotation of the polarization angle of the incident light is also explained by the model combining the birefringence and polarization-dependent loss.

In CRDS, the decay rate of the cavity output power is fitted to a single-exponential decay, which is based on the assumption of single-mode excitation in the cavity. However, the combination of birefringence and polarization-dependent loss leads, for a general state of excitation, to nonexponential decay even when the light is detected without polarization analysis. Also, the effective cavity decay rate can depend strongly on the input polarization state, leading to baseline drifts. In this paper, we have demonstrate that this excess noise can be removed by putting a high-extinction-ratio polarizer in front of the cavity with its angle properly selected.

This work was supported by the University of Virginia. We thank Daniele Romanini for helpful comments on our manuscript.

References and Notes

1. A. O'Keefe and D. A. G. Deacon, "Cavity ring-down optical spectrometer for absorption measurements using pulsed laser sources," *Rev. Sci. Instrum.* **59**, 2544 (1988).
2. D. Romanini and K. K. Lehmann, "Ring-down cavity absorption spectroscopy of the very weak HCN overtone bands with six, seven, and eight stretching quanta," *J. Chem. Phys.* **99**, 6287–6301 (1993).
3. K. K. Lehmann, "Ring-down cavity spectroscopy cell using continuous wave excitation for trace species detection," U.S. patent 5,528,040 (18 June 1996).
4. J. Dudek, P. Rabinowitz, K. K. Lehmann, and A. Velasquez, "Trace gas detection with cw cavity ring-down laser absorption spectroscopy," presented at 52nd Ohio State University International Symposium on Molecular Spectroscopy, Columbus, Ohio, 16–20 June 1997, paper 36 WG05.
5. D. Romanini, A. A. Kachanov, N. Sadeghi, and F. Stoeckel, "Cw cavity ring down spectroscopy," *Chem. Phys. Lett.* **264**, 316–322 (1997).
6. H. Huang and K. K. Lehmann, "Noise in cavity ring-down spectroscopy caused by transverse mode coupling," *Opt. Express* **15**, 8745–8759 (2007).
7. A. E. Siegman, *Lasers*, 4th ed. (University Science Books, 1986), Sec. 21.7.
8. D. Jacob, M. Vallet, F. Bretenaker, A. Le Floch, and M. Oger, "Supermirror phase anisotropy measurement," *Opt. Lett.* **20**, 671–673 (1995).
9. J. L. Hall, J. Ye, and L. Ma, "Measurement of mirror birefringence at the sub-ppm level: proposed application to a test of QED," *Phys. Rev. A* **62**, 013815 (2000).
10. J. Morville and D. Romanini, "Sensitive birefringence measurement in a high-finesse resonator using diode laser optical self-locking," *Appl. Phys. B* **74**, 495–501 (2002).
11. J. Y. Lee, H. W. Lee, J. W. Kim, Y. S. Yoo, and J. W. Hahn, "Measurement of ultralow supermirror birefringence by use of the polarimetric differential cavity ringdown technique," *Appl. Opt.* **39**, 1941–1945 (2000).
12. A. Le Floch and R. Le Naour, "Theoretical existence and experimental evidence of basculating eigenvectors in a Fabry-Perot," *C. R. Acad. Sci. Ser. B* **288**, 225–228 (1979).
13. V. Evtuhov and A. E. Siegman, "A 'twisted-mode' technique for obtaining axially uniform energy density in a laser cavity," *Appl. Opt.* **4**, 142–143 (1965).
14. M. Vallet, F. Bretenaker, A. Le Floch, R. Le Naour, and M. Oger, "The Malus Fabry-Perot interferometer," *Opt. Commun.* **168**, 423–443 (1999).
15. Y. L. Grand and A. Le Floch, "Sensitive dichroism measurements using eigenstate decay times," *Appl. Opt.* **29**, 1244–1246 (1990).
16. R. Engeln, G. Berden, E. van den Berg, and G. Meijer, "Polarization dependent cavity ring down spectroscopy," *J. Chem. Phys.* **107**, 4458–4467 (1997).
17. R. C. Jones, "A new calculus for the treatment of optical systems. I. Description and discussion of the calculus," *J. Opt. Soc. Am.* **31**, 488–493 (1941).
18. J. B. Dudek, P. B. Tarsa, A. Velasquez, M. Wladyslawski, P. Rabinowitz, and K. K. Lehmann, "Trace moisture detection using continuous-wave cavity ring-down spectroscopy," *Anal. Chem.* **75**, 4599–4605 (2003).
19. The output of the cavity for monochromatic excitation will be in a state of definite polarization (i.e., describable by a Jones vector). However, when the finite line width of the excitation source is averaged over, the cavity output will be a partially incoherent superposition of different polarization vectors even if the input is in a definite polarization state independent of frequency.
20. E. Hecht, *Optics* 4th ed. (Addison-Wesley, 2002), p. 376.
21. T. Muller, K. Wiberg, and P. Vaccaro, "Cavity ring-down polarimetry (CRDP): a new scheme for probing circular birefringence and circular dichroism in the gas phase," *J. Phys. Chem. A* **104**, 5959–5968 (2000).
22. C. Z. Tan and J. Arndt, "Wavelength dependence of the Faraday effect in glassy SiO₂," *J. Phys. Chem. Solids* **60**, 1689–1692 (1999).